공학석사학위논문

실제 기체 효과를 고려한 천연가스 터보 익스팬더 유동 해석

Analysis of Real Gas Effects in Natural Gas Turbo-Expanders

2017년 8월

서울대학교 대학원

기계항공공학부

최 윤 정

Abstract

Analysis of Real Gas Effects in Natural Gas Turbo-Expanders

Yun Jung Choi

Department of Mechanical & Aerospace Engineering

Seoul National University

During transport and storage of natural gas, natural gas turbo-expanders are used to throttle the high pressure gas and to increase the system efficiency by extracting additional work. This study reports how real gas effect influence prediction of the flow field in the turbo-expander focusing on mass flow rate and efficiency. The tested thermodynamic gas models include the polytropic ideal gas law (PIG), Peng-Robinson equation of state (PR), and Redlich-Kwong equation of state (RK). Simulations have been performed with Ansys CFX 17.0. and methane has been selected as the working fluid. Real gas equation of state is validated by comparing the calculated compressibility factor with that of measured REFPROP. Simulation with the RK EOS has been selected as the reference. PIG model shows a 13% and 20% difference the mass flow rate and efficiency, respectively. PR and

RK models show similar results, showing less than 2.1% difference in mass flow rate and efficiency. Predicted density determines mass flow rate. With the blocking effect due to separation bubble, the effective area is the smallest in the PIG law and the mass flow rate is also the smallest. The smaller efficiency arises from larger loss. The losses are analyzed at the nozzle, nozzle-impeller interface, and impeller, respectively by entropy generation. With the large expansion ratio, nozzle wake and separation bubble on the impeller suction surface, PIG law shows 3 times larger loss than that of reference. Mass flow rate and efficiency are important design factors, so real gas effects need to be considered for turbo-expander design and analysis.

Keywords: turbo-expander, equation of state, natural gas, methane, CFD, real gas effect, ideal gas

Student Number: 2015-22725

Contents

List of Figures

List of Tables

Nomenclature

A	area (m^2)
A_B	blockage area (m^2)
a	correcting constant for attractive of molecules
b	correcting constant for gas volume
C	absolute velocity (m/s)
Cp	static pressure coefficient
c_p	specific heat capacity at constant pressure (J/kg K)
c_v	specific heat capacity at constant volume (J/kg K)
h_t	total enthalpy (kJ/kg)
P	static pressure (Pa)
R	universal gas constant (8.314J/K mol)
ΔS	entropy generation (J/kg K)
T	temperature (K)
Tc	critical temperature (K)
$\overline{U}$	average velocity (m/s)
Uc	core velocity (m/s)
v	molar volume (m^3/mol)
Z	compressibility factor (K)

Greek

ζ	loss coefficient
η	efficiency
κ	non-centricity of molecules

ρ density (kg/m^3)

Subscripts

1 nozzle inlet

2 nozzle outlet

2' impeller inlet

3 impeller outlet

Chapter 1. Introduction

Reduction in energy costs, eco-friendly policies and continued use of shale gas will increase the importance of natural gas. This makes the process of natural more important, including gas refining, storage, transport, and application. Turbo expanders are widely used in industry to chill the gas or vapor stream, reduce pressure, and obtain mechanical work (Bloch et al. 2001). This paper deals with an expander for throttling high temperature and high pressure gas.

During transport, natural gas is stored in the liquefied state, and it vaporized slightly. For safety and cost, gas is reliquefied or used for the transport engine. A gas expander can be found in the process of depressurizing or methane refrigeration system (MRS) using gaseous natural gas as a coolant.

Computational fluid dynamic (CFD) simulation is usually used to design or analyze turbomachinery flows. In general, polytropic ideal gas (PIG) laws are used. Flow with ideal gas assumption can be different from the actual flow field. In particular, various thermodynamic properties, such as dynamic viscosity and specific heat capacity, are assumed to be constant. This assumption results in inaccurate flow predictions at high pressure.

Hanrinck et al. (2010) investigated real gas effects in a turbine cascade using toluene, R245fa, and steam as working fluids with CFD. In this way, real gas effects have been studied in designing turbine, but not when the working fluid is natural gas. Nasrifar et al. (2006) investigated the accuracy of thermo-physical properties of

natural gas mixtures using 10 different equation of state. Molleson et al. (2005) using natural gas mixtures and Abdi et al. (2010) using methane and carbon dioxide analyzed nozzle flows.

Thus researchers have focused on characterizing the natural gas properties. However, simulations of natural gas flow in turbo-expanders have not yet been reported in the open literature. Therefore, this paper reports on how the three thermodynamic gas models influcence prediction of the flow field in the turbo-expander. Three most widely used thermodynamic models are selected. Three thermodynamic models include the polytropic ideal gas law (PIG), Peng-Robinson equation of state (PR) (Peng and Robinson, 1976), and Redlich-Kwong equation of state (RK) (Redlich and Kwong, 1949).

Chapter 2. Numerical Method

Simulations have been performed with Ansys CFX 17.0. The natural gas of interest has methane greater than 96%. Therefore, methane has been selected as the working fluid. Hanwha Techwin expander geometry has used for expander simulations. The simulation was performed at the design point.

2-1. Mesh quality assessment

Mesh quality assessment was carried out in 3 element numbers. 3 cases are named coarse, mid, and fine. Each value was predicted at the impeller exit and divided by value of fine case.

	Coarse	Mid	Fine
Number of grid elements (million)	0.48	2.14	6.65

Table 2.1. Numerical grid sizes.

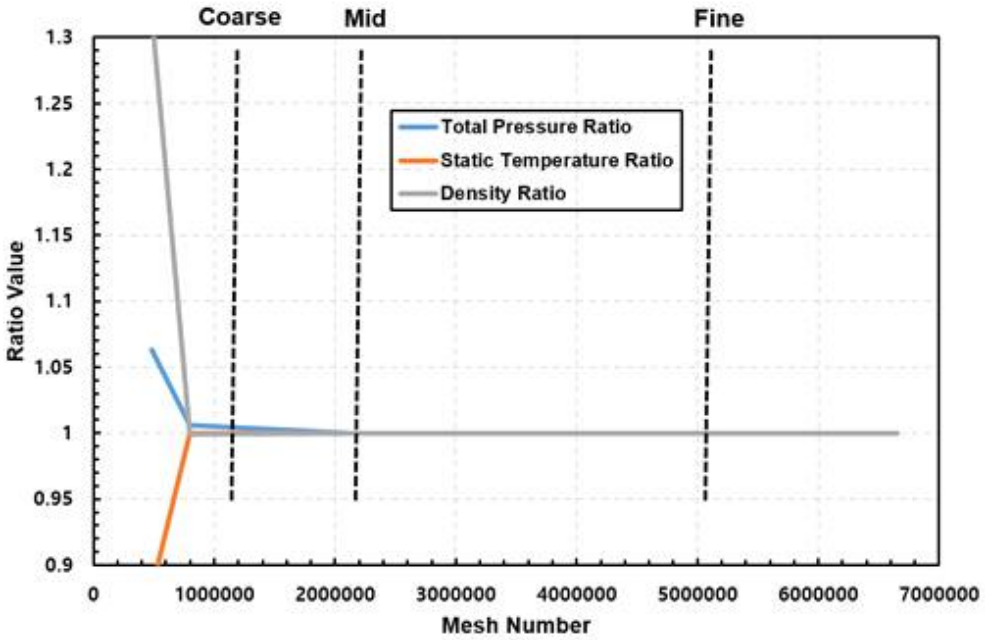

Figure 2.1. Total pressure, static temperature and density ratio depending on grid elements number.

2-2. Solver setup

A steady state simulation is performed. CFD domain is restricted to one passage per row and periodic boundary conditions are used. The CFD domain is also described in Figure 2.2.

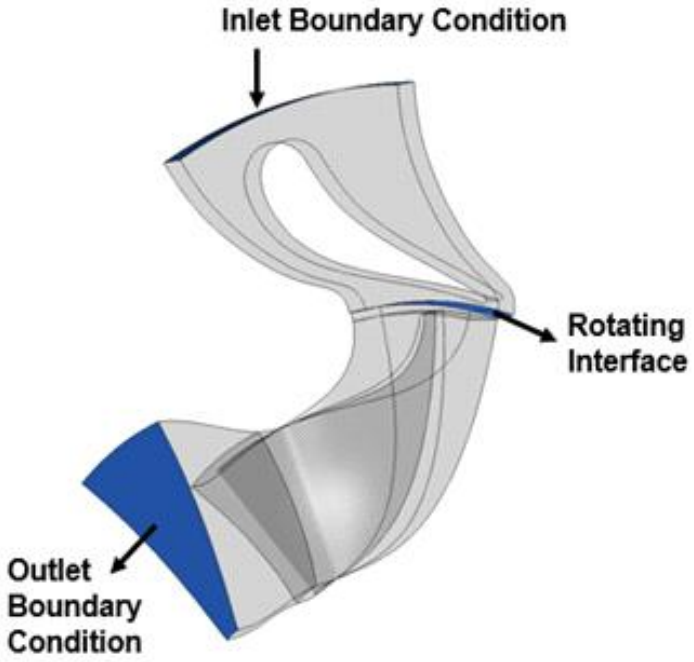

Figure 2.2. CFD domain.

The Flow is modelled as a fully turbulent flow using the shear-stress transport (SST) turbulence model. The total Energy, including viscous work term, is used to calculate heat transfer. All solid walls including nozzle and impeller blades, are rough walls with 19μm roughness. No-slip boundary condition is used for all solid walls. Mixing plane is selected for the rotating interface. Total pressure and total temperature are applied to the inlet boundary condition. Inlet flow direction is normal to inlet plane. Turbulence rate is set at 5%. Average static pressure is applied at the outlet.

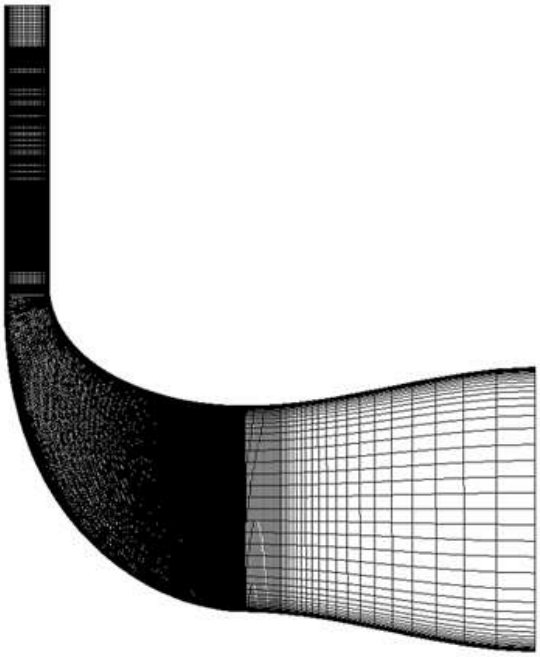

Figure 2.3. Grid generation.

2-3. Equation of state for gases

Equation of state describes the relations among thermodynamic properties. In this study, ideal gas assumption and two equations considering real gas effect have been used.

Polytropic ideal gas law (PIG law)

The PIG law assumes that there is no attraction between gas molecules. It is known that the PIG is well satisfied at low pressures. The PIG equation is:

$$P = \frac{RT}{v} \tag{2.1}$$

where,

P: pressure

R: universal gas constant

T: temperature

v: molar volume

Molar volume is volume occupied by one mole of a substance. In the PIG, specific heat ratio, dynamic viscosity, and thermal conductivity are assumed to be constant.

Real gas law

Real gas law considers compressibility effect. Generally, compressibility factor is expressed as Z, the equation is:

$$Z = \frac{RT}{Pv} \tag{2.2}$$

where,

Z: compressibility factor

P: pressure

R: universal gas constant

T: temperature

v: molar volume

Z has a value of 1 in the PIG law and is used to describe the deviation of a real gas from the ideal gas.

The Redlich-Kwong (RK) and the Peng Robinson (PR) Equations of State are most commonly used and are known to be accurate. (Nasrifar et al, 2006)

The RK equation of state is:

$$P = \frac{RT}{v} - \frac{a\alpha(T)}{v(v+b)} \tag{2.3}$$

where,

P: pressure

R: universal gas constant

T: temperature

v: molar volume

a: correcting constant for attractive of molecules

b: correcting constant for gas volume

$\alpha(T)$: $T^{-0.5}$

The PR equation of state is:

$$P = \frac{RT}{v} - \frac{a\beta(T)}{v(v+b)+b(v-b)} \tag{2.4}$$

where,

P: pressure

R: universal gas constant

T: temperature

v: molar volume

a: correcting constant for attractive of molecules

b: correcting constant for gas volume

$\beta(T)$: $\left[1+\kappa(1-(\frac{T}{T_c})^{0.5})\right]^2$

κ: non-centricity of molecules

T_c: critical temperature

CFD validation

The above three equations have been internally coupled to the CFD solver to calculate the thermodynamic properties of natural gas. For real gas EOS, zero pressure coefficient of specific heat capacity is used as reference. This variable is calculated as a fourth order polynomial [2].

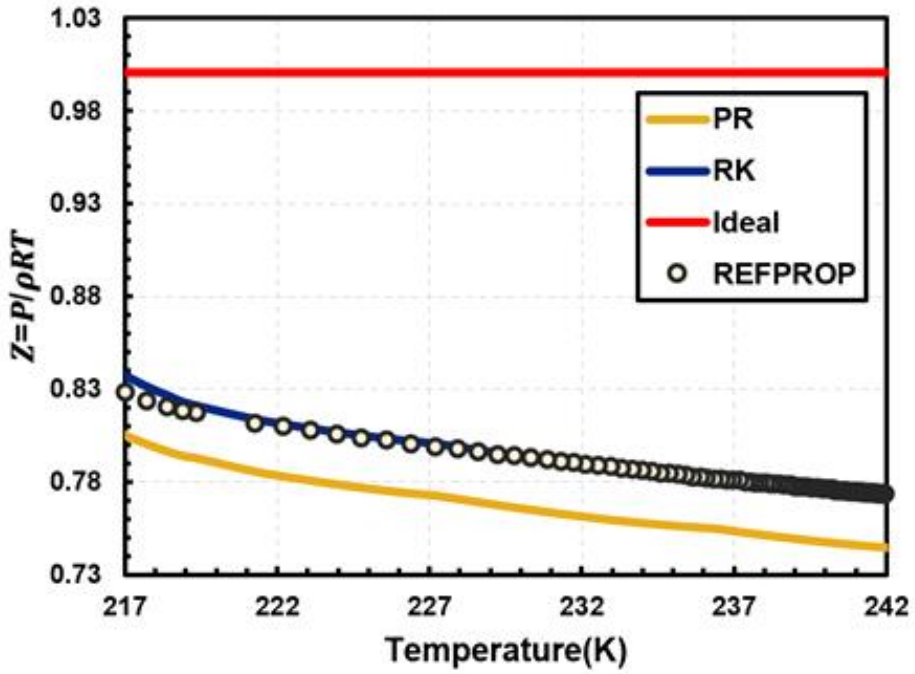

Figure 2.4. Compressibility factor for three thermodynamic models versus REFPROP data.

Figure 2.4. shows the compressibility factor in terms of temperature predicted by the three thermodynamic models in turbo-expander nozzle flow. Z of the PIG law remains constant at 1, and RK EOS and PR EOS cases have smaller values. Compared with REFPROP measured data, the Z value from the RK EOS has the best fit. Therefore, the RK EOS case has been selected used as the reference case.

Chapter 3. Results and Discussion

3-1. Mass flow rate

	PIG law	RK EOS	PR EOS
Mass flow rate [kg/s]	0.661	0.764	0.779

Table 3.1. Mass flow rate.

The mass flow rate of the PIG is 13% less and the mass flow rate of the PR EOS is 3% higher than the RK EOS flow rate. The relative big difference of the PIG law is due to the predicted density difference and the blockage effect of the separation bubble on the impeller blade.

Density

The temperature predicted by the PIG law is higher than the reference. The temperature of PR EOS is 1.1% lower than that of reference and the difference is small. But the temperature of the PIG law is 11.8% higher than that of reference. Density value is small due to high temperature. The density values are also calculated differently depending on the equation used even at the same state. Therefore, the PIG law density shows 13% error when compared to REFPROP data at the same state. With the same volume, the mass

flow rate of PIG law is lower.

	PIG law	RK EOS	PR EOS
Temperature [K]	179.9	161.8	160
Density [kg/m^3]	14.59	20	20.7
REFPROP density [kg/m^3]	16.74	19.9	20.36
Density error [%]	20.36	0.5	1.67

Table 3.2. Predicted temperature and density versus REFPROP.

Blockage Effect

Table 3.3. lists the blockage area ratio for the three thermodynamic models. The PIG law case has the largest blockage effect.

$$\frac{A_B}{A} = 1 - \frac{\overline{U}}{U_c} \tag{3.1}$$

where,

A_B: blockage area

A: area

$\overline{U}$: average velocity

U_c: core velocity

	PIG law	RK EOS	PR EOS
$\frac{A_B}{A}$	0..07	0.038	0.031

Table 3.3. Blockage area ratio.

3-2. Efficiency

Total-to-static efficiency is:

$$\eta_{ts} = \frac{actual\,work\,(h_{t,inlet} - h_{t,outlet})}{ideal\,work\,(h_{t,inlet} - h_{ideal,\,outlet})} \tag{3.2}$$

where,

h_t: total enthalpy

h_{ideal}: isentropic enthalpy

Total-to-static efficiency is the ratio of the actual work to the ideal work. PIG law case has larger ideal work and larger real work than reference case. However, the loss of the PIG law case is much greater than the RK case, so the efficiency is lower. The PR case has the smallest ideal work and the actual work. However, the

efficiency is the highest, because the ratio of loss to actual work is the smallest of the three cases. That is, difference loss causes different efficiency. Since the domains of the simulation are assumed to be adiabatic, loss generation is explained by entropy generation.

	PIG law	RK EOS	PR EOS
Ideal work [kJ/kg]	187.31	121.51	114.82
Actual work [kJ/kg]	132.63	106.57	102.92
Efficiency [%]	70.8	87.7	89.6
Loss [kJ/kg]	54.68	14.94	11.9
Loss/actual work	0.41	0.14	0.116

Table 3.4. Work, loss and efficiency.

The geometry is divided into three parts: the nozzle, the part between nozzle and impeller, and the impeller. PIG law case has the largest entropy generation at every location. The difference between RK EOS and PR EOS for total entropy generation is 7.6%. The difference in entropy generation is the lowest in the nozzle, then nozzle-impeller interface, then impeller.

	PIG law	RK EOS	PR EOS
ΔS nozzle [J/kgK]	33.91	24.58	23.21
ΔS nozzle−impeller interface [J/kgK]	30.53	18.87	17.4
ΔS impeller [J/kgK]	56.9	17.73	15.93
ΔS total [J/kgK]	121.35	61.185	56.554

Table 3.5. Entropy generation in all locations.

Nozzle

The nozzle part is from the nozzle blade inlet to nozzle blade outlet. The nozzle blade entry before the CFD domain inlet is not covered.

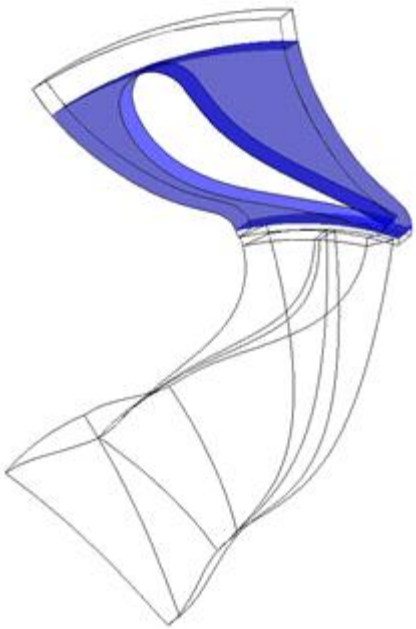

Figure 3.1. Nozzle geometry.

Table 3.6. shows the thermodynamic properties at the nozzle inlet and outlet. Pressure and temperature are similar for all three equations of state. But at the nozzle outlet, the PIG law case has lower pressure and higher temperature. According to the equation (3.3), the lower pressure and the higher temperature results in the larger entropy generation. In the case of PIG law, the value of c_v is constant. In RK EOS and PR EOS, the value of c_v changes with temperature. The c_v value in the temperature range of the nozzle is larger with the real gas EOS than constant value of PIG law. However, the entropy generation is largest with the PIG law because the pressure is 10% lower than the reference.

	PIG law	RK EOS	PR EOS
Pressure 1 [Mpa]	6.18	6.158	6.159
Temperature 1 [K]	242.7	242.6	242.6
Pressure 2 [Mpa]	2.6	2.88	2.94
Temperature 2 [K]	201	198.1	198.2
ΔS nozzle [J/kgK]	33.91	24.58	23.21

Table 3.6. Predicted pressure and temperature at nozzle inlet and outlet.

Entropy generation is:

$$\Delta S = c_v \ln\left(\frac{T_2}{T_1}\right) - R \ln\left(\frac{P_2}{P_1}\right) \tag{3.3}$$

where,

c_v: specific heat capacity at constant volume

P: pressure

R: universal gas constant

T: temperature

To determine if there is an additional reason for the entropy generation difference, the loss by total pressure is calculated. In all three cases, the difference is less thann 1%. Therefore, the difference in entropy generation in the nozzle part is due to the difference in the predicted properties rather than the loss due to the special phenomenon.

$$\zeta = \frac{P_{01} - P_{02}}{\frac{1}{2}\rho_2 C_2^2} \tag{3.5}$$

where,

P_0: total pressure

1: nozzle inlet

2: nozzle outlet

ρ: density

C: absolute velocity

	PIG law	RK EOS	PR EOS
Loss coefficient ζ	0.1491	0.1476	0.14648

Table 3.7. Loss coefficient in nozzle.

Nozzle-impeller interface

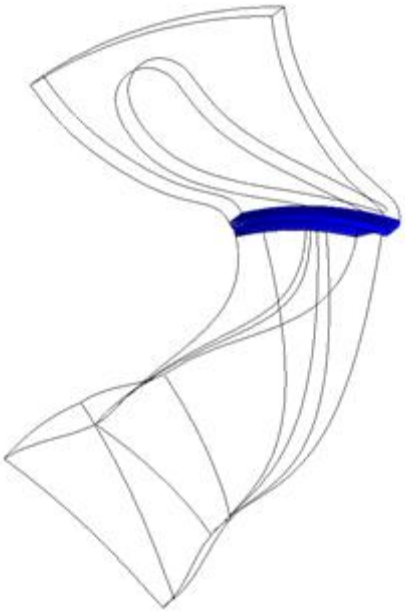

Figure 3.2. Nozzle-impeller interface geometry.

The nozzle-impeller interface part is from immediately after the nozzle blade to the inlet of the impeller blade. Compared to other parts, the space where the flow passes is short and the pressure change is small. On the other hand, generated entropy is quite large. In the nozzle, PIG law and RK EOS have 38%, PR EOS and RK EOS have 5.5% error. However, PIG law and RK EOS have 61.8%, PR EOS and RK EOS have 7.8% in the nozzle-impeller interface.

	PIG law	RK EOS	PR EOS
ΔS nozzle [J/kgK]	33.91	24.58	23.21
Ratio of difference with RK EOS [%]	38	0	5.5
ΔS nozzle−impeller interface [J/kgK]	30.53	18.87	17.4
Ratio of difference with RK EOS [%]	61.8	0	7.8

Table 3.8. Entropy generation difference.

As in the case of the nozzle, the loss coefficient was calculated in the nozzle-impeller interface. Compared with the nozzle with less than 1% difference, the absolute value is small, but the difference of loss coefficient between PIG law and RK EOS is more than 4%. This difference is due to the mixing loss which also caused additional entropy generation.

$$\zeta = \frac{P_{02} - P_{02'}}{\frac{1}{2}\rho_{2'} C_{2'}^2} \tag{3.6}$$

where,

P_0: total pressure

2: nozzle outlet

2': impeller inlet

ρ: density

C: absolute velocity

	PIG law	RK EOS	PR EOS
Loss coefficient ζ	0.03558	0.0298	0.02862

Table 3.9. Loss coefficient in nozzle-impeller interface.

Figure 3.3 shows the nozzle shape. The number of nozzle blades and impeller blades are difference, so the distance of one passage is different. In order to compare the velocity of the nozzle outlet on the same scale, the nozzle blade outlet was set to line 1 and the line before the rotating part was set to line 2. A nozzle trailing edge is at near zero of normalized pitch.

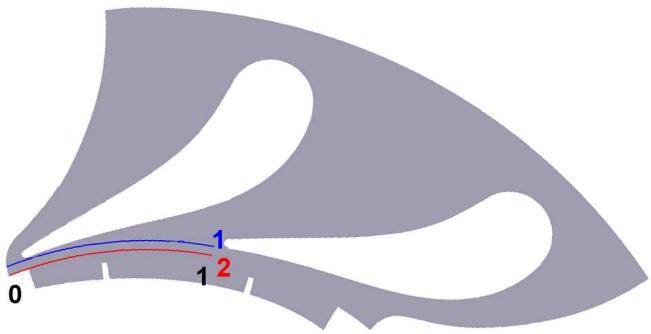

Figure 3.3. Wake detection position.

In Figure 3.4 and 3.5, the velocity distribution in line 1 and 2 are plotted. Wake is observed near the nozzle trailing edge, but

velocity becomes uniform as the flow mixes. PIG law has wider and deeper wake than RK EOS and PR EOS. The larger the wake size, the greater the mixing loss required to make the velocity uniform. In the PIG law case, this large mixing loss due to nozzle blade wake causes larger entropy generation.

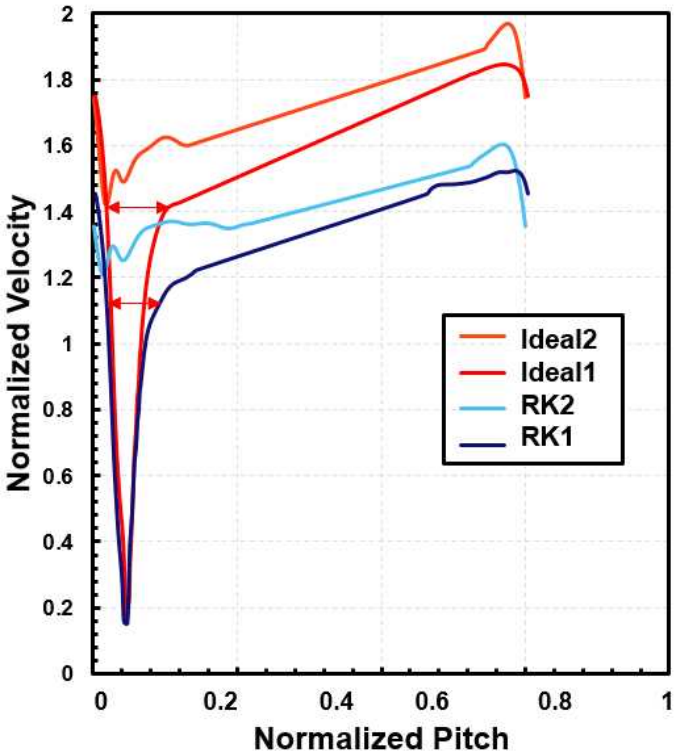

Figure 3.4. Velocity distribution at nozzle outlet (PIG law vs. RK EOS).

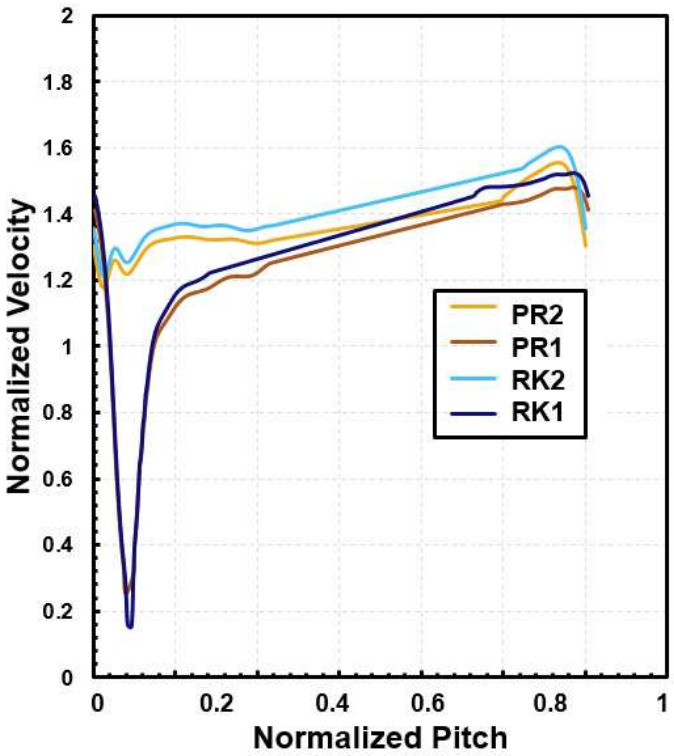

Figure 3.5 Velocity distribution at nozzle outlet (PR EOS vs. RK EOS).

Impeller

The impeller part is from the inlet to the outlet of the impeller blade. It is shown in blue color in Figure 3.6. The diffuser part after impeller is not covered.

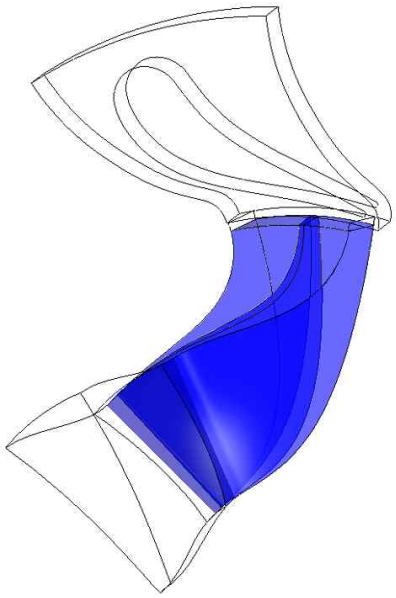

Figure 3.6. Impeller geometry.

The entropy generation of PIG law in the impeller part is about 3.6 times larger than that of PR EOS and 3 times larger than that of RK EOS. The loss coefficient of the PIG law is more than 2.5 times greaterthan that of RK EOS. This is also consistent with the entropy generation. Therefore, the difference in loss can be also explained by the cause of the difference in entropy generation.

	PIG law	RK EOS	PR EOS
ΔS Impeller	56.9	17.73	15.93

Table 3.10. Entropy generation in impeller.

Unlike axial turbomachinery, enthalpy loss should be taken into account when calculating loss in radial turbomachinery with radius change. The loss coefficient is:

$$\zeta = \frac{P_{T2'} - P_{T3}}{P_{T3} - P_3} \tag{3.7}$$

$$P_T = \rho \left(\frac{T_T}{T}\right)^{\frac{\gamma}{\gamma-1}} \tag{3.8}$$

$$T_T = \frac{h_t}{c_p} \tag{3.9}$$

$$\gamma = \frac{c_p}{c_v} \tag{3.10}$$

where,

2': impeller inlet

3: impeller outlet

ρ: density

h_t: total enthalpy

c_p: specific heat capacity at constant pressure

	PIG law	RK EOS	PR EOS
Loss coefficient ζ	2.339	0.9416	0.6923

Table 3.11. Loss coefficient in impeller.

The most noticeable phenomenon in the flow through the impeller is the separation bubble on impeller blade suction side. Figures show chordwise pressure distribution on impeller blade at the mid span of PIG law, RK EOS and PR EOS, respectively. The pressure coefficient is:

$$C_p = \frac{P - P_3}{\frac{1}{2}\rho_3 U_3^2} \tag{3.11}$$

where,

3: impeller outlet

C_p: pressure coefficient

ρ: density

U: velocity

The upper line is the pressure side and the lower line is the suction side. PR EOS shows a graph of the same trend as RK EOS and the pressure coefficient decreases on both sides. However, there is a slight increase followed by a plateau on the suction side in the case of PIG law. This plateau indicates flow separation. Velocity vectors are drawn in the impeller for visualization. Separation bubble also occurs in RK and PR EOS, its size is significantly smaller than that of PIG law.

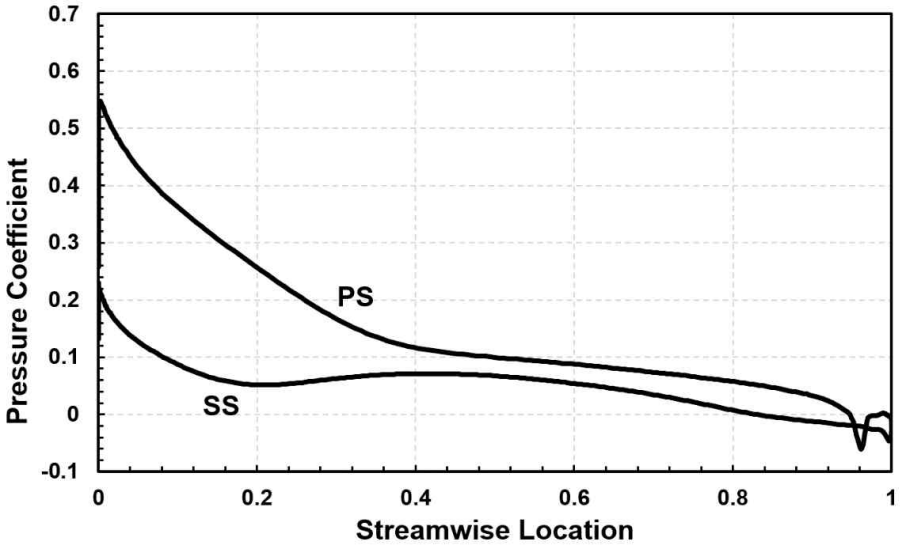

Figure 3.7. Chordwise pressure distribution on the impeller blade (PIG Law, Mid Span).

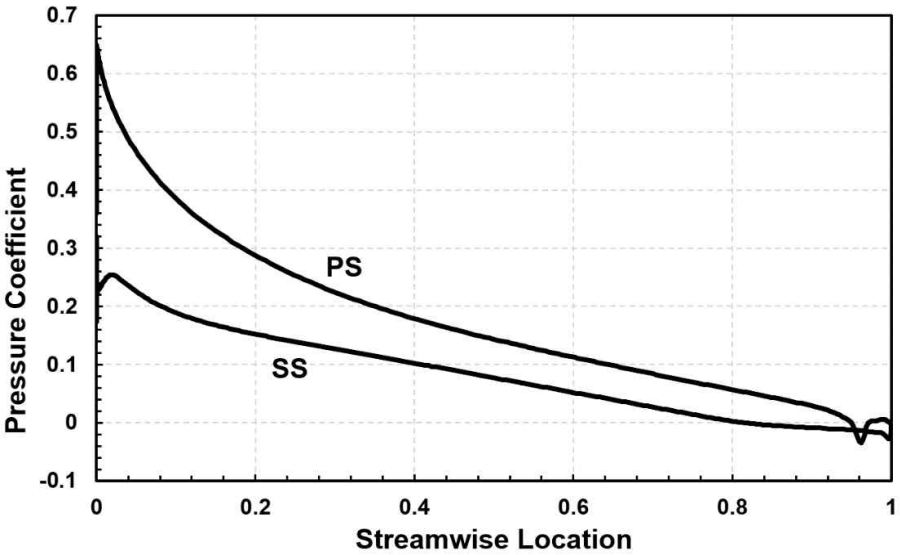

Figure 3.8. Chordwise pressure distribution on the impeller blade (RK EOS, Mid Span).

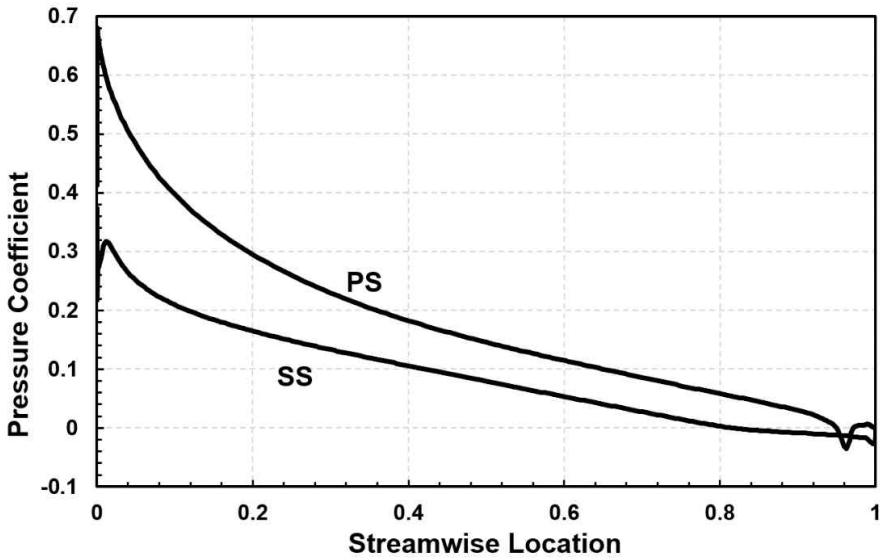

Figure 3.9. Chordwise pressure distribution on the impeller blade (PR EOS, Mid Span).

Figures show the velocity vectors of the flow through impeller at the mid span of PIG, RK EOS and PR EOS, respectively. Vector is the non-dimensionalized velocity by the impeller tip speed. The scale is unified for three thermodynamic cases. In the PIG law case, there was a separation bubble of 37.14% of impeller chord length size. Separation bubbles are also observed in RK EOS and PR EOS cases. The separation bubble sizes were 9.16% and 6.8% of impeller chord length, respectively.

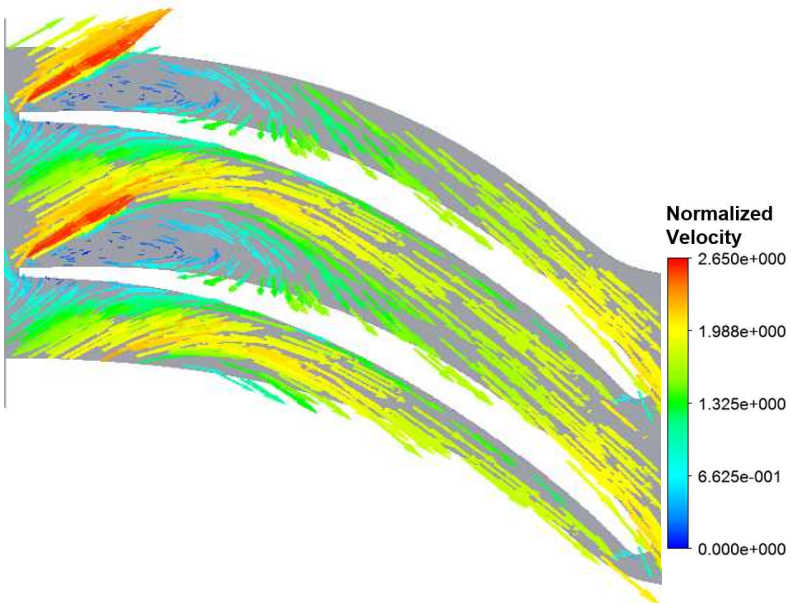

Figure 3.10. Velocity vector visualization (PIG Law, Mid Span).

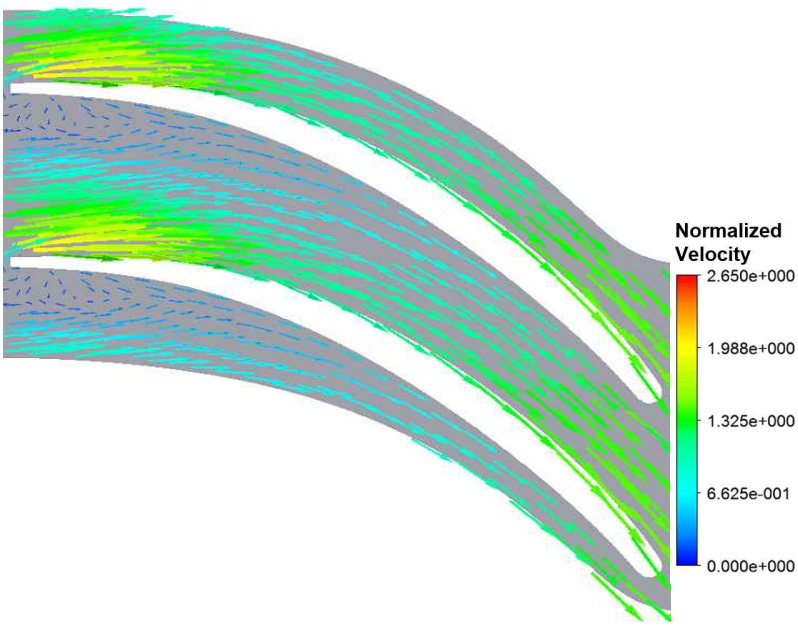

Figure 3.11. Velocity vector visualization (RK EOS, Mid Span).

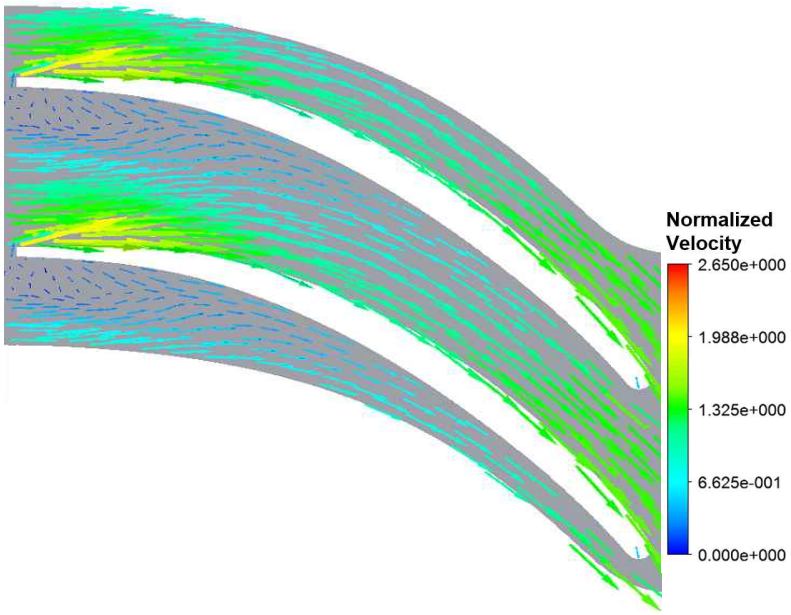

Figure 3.12. Velocity vector visualization (PR EOS, Mid Span).

The velocity vector was visualized in the near hub and near shroud in order to investigate the separation bubble in the PIG law case. The non-dimensional velocity scale is the same. Separation bubble is observed in near hub and shroud as in the mid span. The geometry used in this research has no tip leakage because tip clearance is assumed to be zero. So it is observed that the flow is reflected by hitting the hub and the shroud wall. Except for this, a separation bubble was observed in the same form as in the mid span, indicating a separation bubble is a two-dimensional phenomenon.

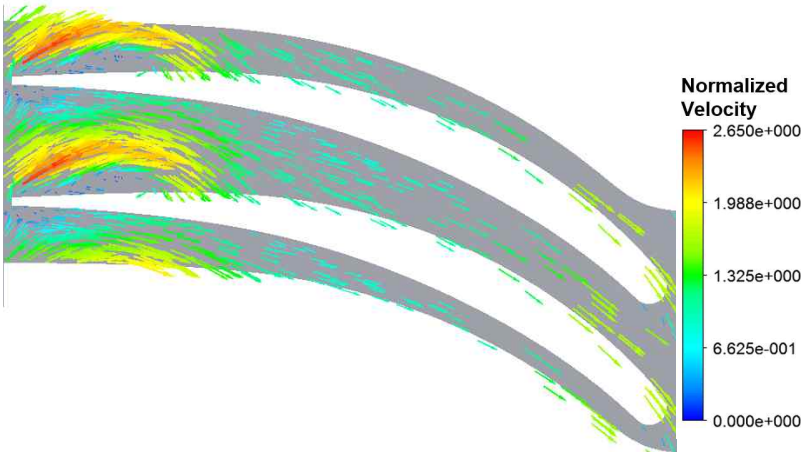

Figure 3.13. Velocity vector visualization (PIG Law, Near Hub).

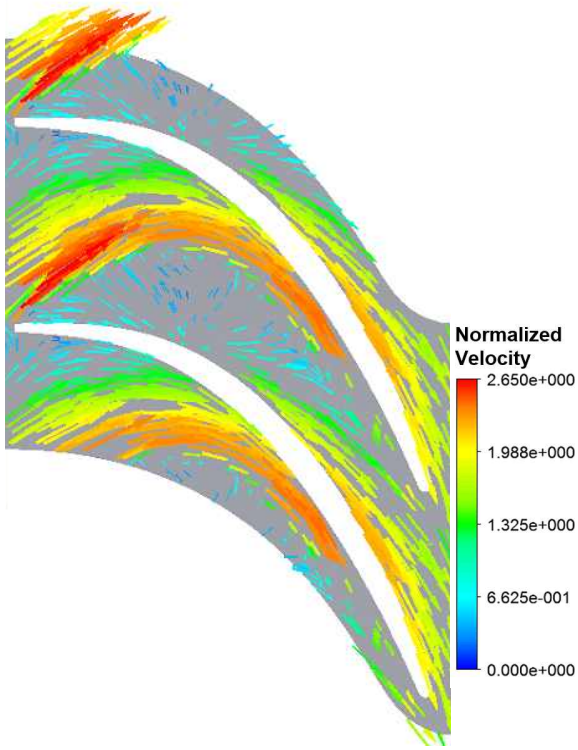

Figure 3.14. Velocity vector visualization
(PIG Law, Near Shroud).

To confirm the separation bubble causes the entropy generation, the velocity vector and entropy generation are drawn together. Black arrows are velocity vector and contour is entropy generation. Contour line collocates with separation bubble. More entropy generated through separation bubble. In the case of RK EOS and PR EOS, the entropy generation on the suction side with a small separation bubble was found to be larger than that of the mid passage.

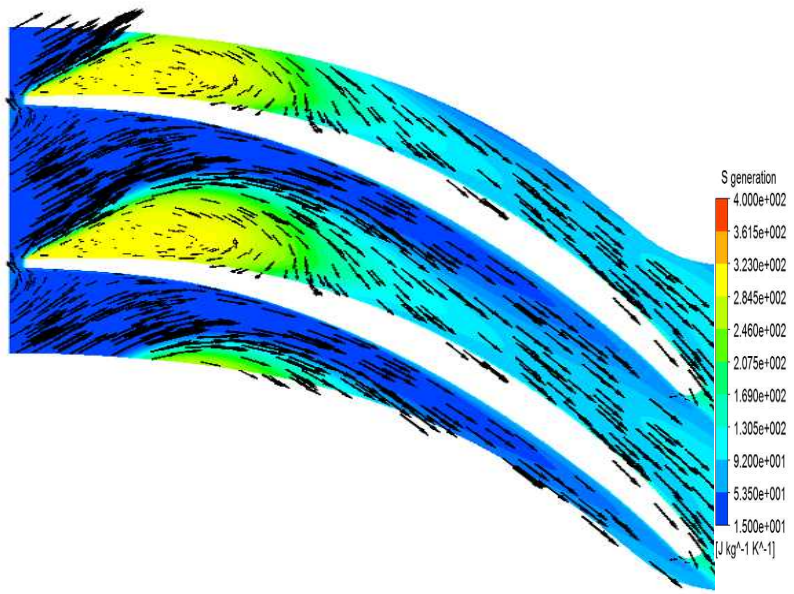

Figure 3.15. Entropy generation with velocity vector (PIG law, Mid span).

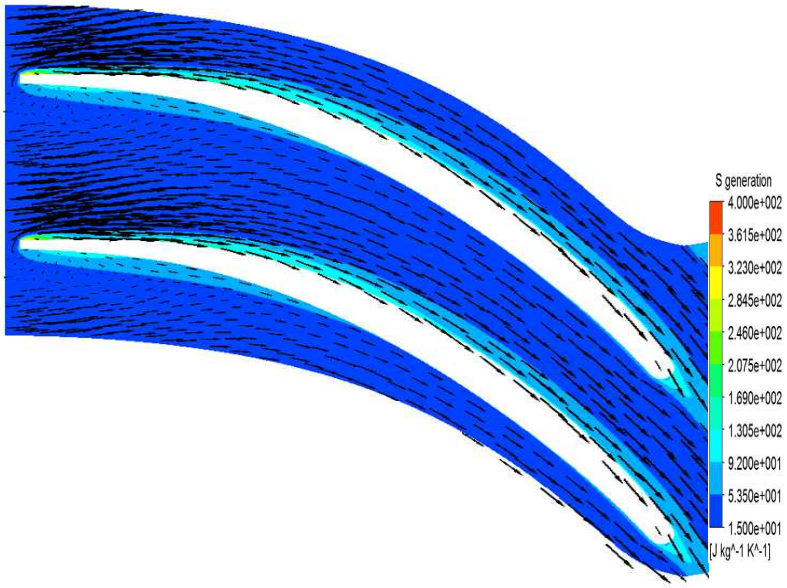

Figure 3.16. Entropy generation with velocity vector (RK EOS, Mid span).

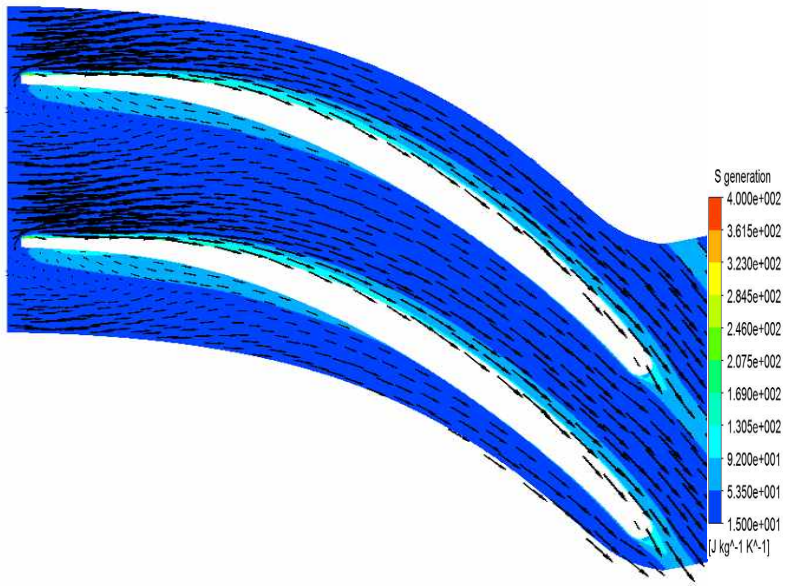

Figure 3.17. Entropy generation with velocity vector (PR EOS, Mid span).

Discuss why the separation bubble size is different in the three EOS, especially the largest separation bubble in the PIG law. The Separation bubble size depends on the incidence angle and the Reynolds number. The size of the separation bubble is proportional to the incidence angle, and inversely proportional to Reynolds number. The incidence angle of the impeller is very large in PIG law. This is shown through the velocity triangle in Figure 3.18, 3.19 and 3.20. RK EOS has an incidence angle of 7.7° and PR EOS has an incidence angle of 0.9°. As a result, the separation bubble is larger at RK EOS than at PR EOS.

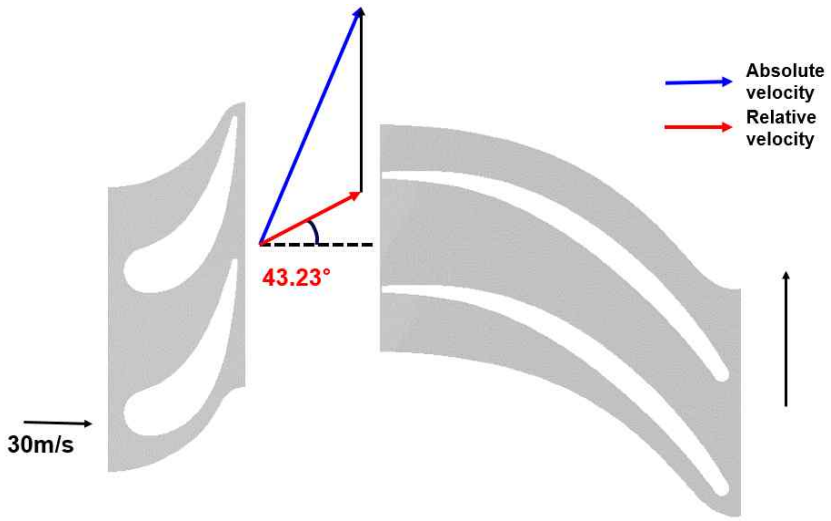

Figure 3.18. Velocity triangle and incidence angle (PIG law).

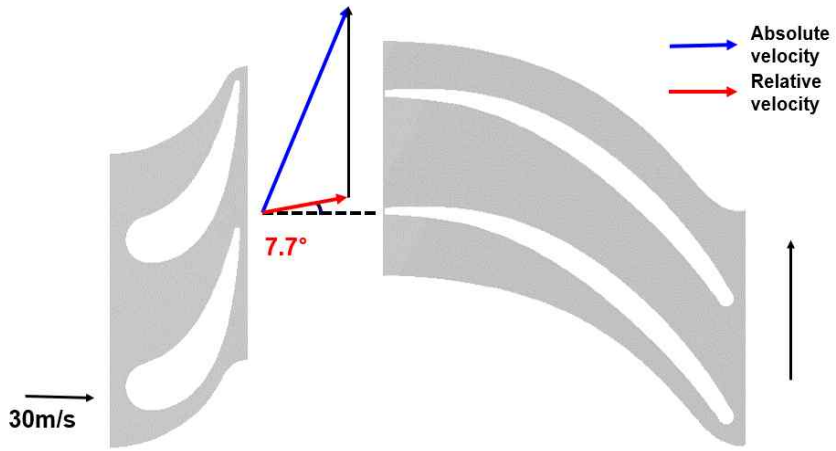

Figure 3.19. Velocity triangle and incidence angle (RK EOS).

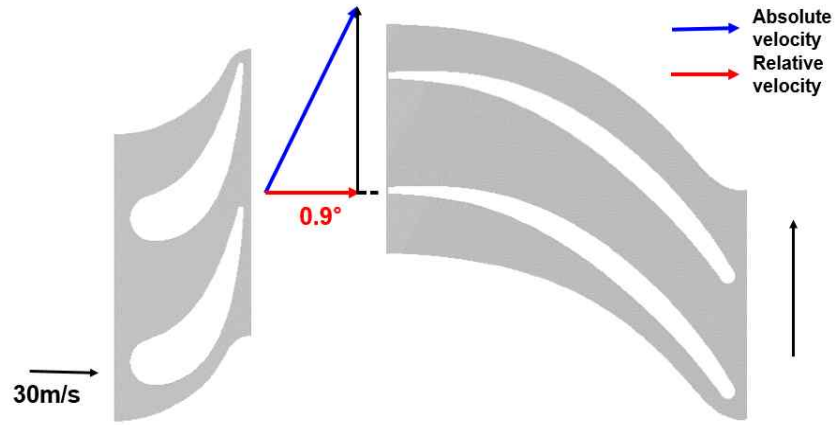

Figure 3.20. Velocity triangle and incidence angle (PR EOS).

Incidence angle is the same for nozzles in three equations of state. The total pressure and static pressure values are similar to

meet the inlet and outlet conditions. Because of this, the dynamic term should be same in all three cases. However, since the density values calculated by the equations are different, the lower the density, the greater the absolute velocity is to compensate. The blade speed is the same because three cases have the same rotating speed with the same radius. Absolute velocity and blade speed determine the relative velocity magnitude and incidence angle to the impeller inlet. The difference in incidence angles by different absolute velocity values is shown in Figure 3.21.

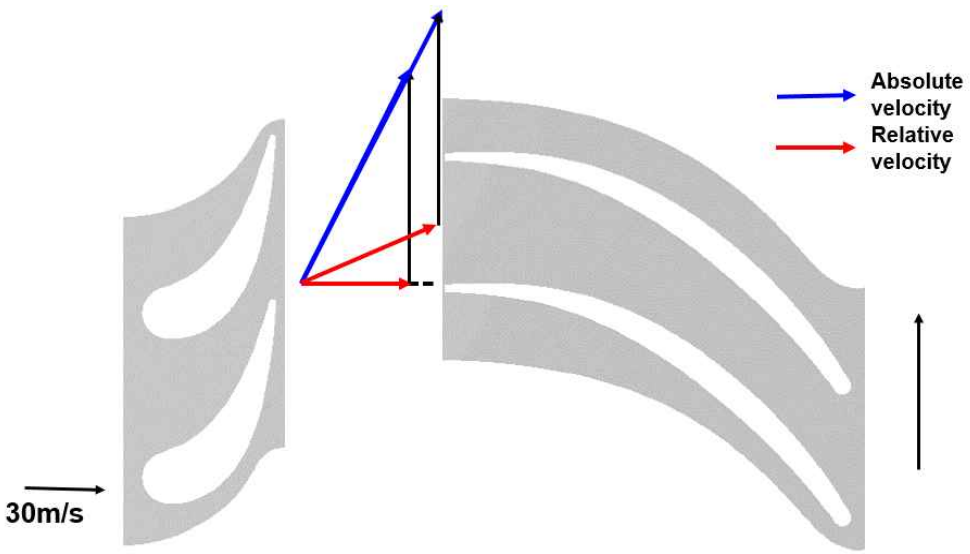

Figure 3.21 Incidence angle depending on absolute velocity.

	PIG law	RK EOS	PR EOS
Total pressure [Mpa]	5.64	5.63	5.63
Static pressure [Mpa]	2.3	2.55	2.6
Density [kg/m^3]	22.22	32.59	34.67
Absolute velocity [m/s]	450.444	366.645	353.2
Incidence angle [°]	43.23	7.7	0.9

Table 3.12. Parameters of incidence angle.

Now discuss the Reynolds number effect. Dynamic viscosity is constant in PIG law. In RK EOS and PR EOS, the dynamic viscosity value changes with temperature and is smaller than the PIG value. The dynamic viscosity of the PR EOS is better matched to that by REFPROP at that pressure and temperature. Also multiple of density and velocity of PIG law is smaller than the other two EOS. The smaller the Reynolds number is, the larger the separation bubble becomes.

	PIG law	RK EOS	PR EOS
Velocity [m/s]	169.2	151.2	150.2
Density [kg/m^3]	14.59	20	20.7
Velocity* Density	2468.6	3024	3109.14
Dynamic Viscosity[Pa*s]	1.11E-5	9.75E-6	6.25E-6
Reynolds number	9.3E+6	1.3E+7	1.9E+7

Table 3.13. Parameters of Reynolds number.

Chapter 4. Conclusions

(1) Natural gas turbo-expander flow has been numerically investigated for the first time with PIG law and real gas EOS.

(2) Difference in the predicted mass flow rates arise from density difference calculated from each equation and blockage effect due to the separation bubble on blade suction side.

(3) Difference in efficiency results from the loss difference which is explained by entropy generation.

(4) Difference in entropy generation comes from predicted properties difference in nozzle, mixing loss due to nozzle blade wake in nozzle-impeller interface, and separation bubble on blade suction side in impeller.

(5) Real gas effects need to be considered for turbo-expander design and analysis.

References

[1] Abdi, M.A. Jassim, E. Haghighi, M. Muzychka, Y. (2010): "Applications of CFD in Natural Gas Processing and Transportation". INTECH, chapter 2.3.1.

[2] Ansys CFX-Solver Theory Guide.

[3] Bloch, H.P. Soares, C. (2001): "Turboexpanders and Process Applications", Gulf Professional Publishing.

[4] Colonna, P. Rebay, S. Hanrink, J. Guardone, A. (2006): "Real-Gas Effects in ORC Turbine Flow Simulations: Influence of Thermodynamic Models on Flow Fields and Performance Parameters", European Conference on Computational Fluid Dynamics ECCOMAS CFD 2006, pp. 1-18.

[5] Denton, J.D. (1993): "Loss Mechanisms in Turbomachines". Journal of Turbomachinery, The 1993 IGTI Scholar Lecture, Vol. 115, pp. 621-656.

[6] Greitzer, E.M. Tan, C.S. Graf, M.B. (2004): "Internal Flow: Concepts and Applications", Campridge University Press, pp. 217-277.

[7] Harinck, J. Colonna, P. Guardone, A. Rebay, S. (2010): "Influence of Thermodynamic Models in Two-Dimensional Flow Simulations of Turboexpanders". Journal of Turbomachinery, Vol. 132, pp.011001-1-011001-17.

[8] Hrgian, A.Kh, (1958): "Fizika atmosfery (Physics of the Atmosphere), Moscow:Fizmatlit.

[9] Japikse, D. Baines, N.C. (1994): "Introduction to Turbomachinery", Concepts ETI, Inc.

[10] Lemmon, E.W. Huber, M.L. McLinden, M.O. (2013): “NIST Reference Fluid Thermodynamic and Transport Properties-REFPROP”, NIST standard Reference Database 23, Version 9.1, User’s Guide.

[11] Molleson, G.V. Stasenko, A.L. (2005): “An Axisymmetric Flow of a Mixture of Real Gases with a Condensing Component”. Teplofizika Vysokikh Temperatur, Vol. 43(3), pp.422-430.

[12] Moustapha, H. Zelesky, M.F. Baines, N.C. Japikse, D. (2003): “Axial and Radial Turbines”, Concepts NRECD, pp. 31-51, 199-206.

[13] Nasrifar, K.H. Bolland, O. (2006): “Prediction of thermodynamic properties of natural gas mixtures using 10 equations of state including a new cubic two-constant equation of state”. Journal of Peroleum Science and Engineering, Vol 51, pp. 253-366.

[14] Patel, V.P. Kimmel, H.E. (2011): “Fifteen Years of Field Experience in LNG Expander Technology”, First Middle East Turbomachinery Syposium.

[15] Peng, D.Y. Robinson, D.B. (1976): “A new two-constant equation ot state”.Industrial and Engineering Chemistry Fundamentals, Vol. 15, pp.59-64.

[16] Redlich, O. Kwong, N.S. (1949): “On the thermodynamics of solutions. V. An equation of state. Fugacities of gaseous solutions”. Chemical Reviews, Vol. 44 (1), pp. 233-244.

요약문(국문초록)

실제 기체 효과를 고려한 천연가스 익스팬더 유동 해석

최 윤 정
기계항공공학부
서울대학교

천연 가스의 운송 및 저장 중에 천연 가스 터보 익스팬더를 사용하여 고압가스를 감압하고 추가적인 일을 얻어 시스템 효율을 높인다. 본 연구에서는 천연가스 내부 유동에 대한 수치해석을 수행하였다. 실제 기체 효과가 유량과 효율에 미치는 영향을 분석하기 위해 이상기체 상태방정식과 실제 기체 효과를 고려한 Redlich-Kwong (RK) 와 Peng-Robinson (PR) 상태방정식을 사용하였다. 시뮬레이션은 Ansys CFX 17.0으로 수행되었으며 작동 유체로 메탄을 사용하였다. 계산된 메탄의 압축 계수와 측정된 REFPROP 압축 계수 비교를 통해 실제 기체를 고려한 상태방정식이 실제와 일치함을 검증하였다. 그 중 실제 기체 행동과 가장 유사한 RK 상태방정식을 기준으로 선정하였다. 유량은 이상기체 상태방정식이 RK 상태방정식에 비해 13% 작고 PR 상태방정식에서 RK 상태방정식에 비해 2% 크다. 같은 부피의 형상에서 예측된 밀도가 이상기체, RK, PR 상태방정식 순서대로 작으므로 유량도 같은 순

서대로 작다. 또한 물리적으로는 분리현상이 차단 효과를 야기하며 이상기체 상태방정식에서 유효 넓이가 가장 작아 유량 역시 가장 작다. 세 상태방정식에서 효율의 차이는 손실의 차이로 설명된다. 손실이 가장 큰 이상기체 상태방정식이 효율이 가장 낮으며 RK 상태방정식과 비교했을 경우 20% 낮다. 손실은 생성된 엔트로피와 일치하며 각각 노즐, 노즐-임펠러 인터페이스, 임펠러에서 분석하였다. RK와 PR 상태방정식의 유동은 비슷하나 이상기체 상태방정식에서 팽창비와 노즐 후류 크기가 크고 임펠러 흡입면에서 분리 (separation bubble)가 관찰된다. 효율과 유량은 중요한 디자인 요소이므로 실제 기체 효과가 고려되어야 한다.

주 요 어: 터보 익스팬더, 상태방정식, 실제 기체 효과, 이상기체, 천연가스, 메탄, 수치해석

학 번: 2015-22725